Engineering Structures 279 (2023) 115429

Contents lists available at ScienceDirect

Engineering Structures

journal homepage: www.elsevier.com/locate/engstruct

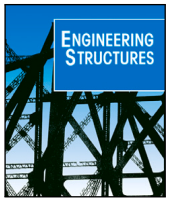

Dynamic testing and numerical modelling of a pedestrian timber bridge at different construction stages

Jens Bergenudd *, Jean-Marc Battini, Roberto Crocetti, Costin Pacoste

Division of Structural Engineering and Bridges, KTH Royal Institute of Technology, Brinellvägen 23, Stockholm, 100 44, Sweden

ARTICLE INFO

Keywords:
Pedestrian bridge
Timber
Railings
Asphalt
Dynamic analysis
Finite element modelling

ABSTRACT

This article studies the dynamic properties of a single span pedestrian timber bridge by in-situ testing and numerical modelling. The in-situ dynamic tests are performed at four different construction stages: (1) on only the timber structure, (2) on the timber structure with the railings, (3) on the timber structure with railings and an asphalt layer during warm conditions and (4) same as stage 3 but during cold conditions. Finite element models for the four construction stages are thereafter implemented and calibrated against the experimental results. The purpose of the study is to better understand how the different parts of the bridge contribute to the overall dynamic properties. The finite element analysis at stage 1 shows that longitudinal springs must be introduced at the supports of the bridge to get accurate results. The experimental results at stage 2 show that the railings contributes to 10% of both the stiffness and mass of the bridge. A shell model of the railings is implemented and calibrated in order to fit with the experimental results. The resonance frequencies decrease with 10–20% at stage 3 compared to stage 2. At stage 3 it is sufficient to introduce the asphalt as an additional mass in the finite element model. For that, a shell layer with surface elements is the best approach. The resonance frequencies increase with 15–30% between warm (stage 3) and cold conditions (stage 4). The stiffness of the asphalt therefore needs to be considered at stage 4. The continuity of the asphalt layer could also increase the overall stiffness of the bridge. The damping ratios increase at all construction stages. They are around 2% at warm conditions and around 2.5% at cold conditions for the finished bridge.

1. Introduction

Timber is an important construction material in order to reach a sustainable future. Transports can be shortened if there is local availability of timber and construction time can be reduced since the low mass of timber allows for a high degree of pre-fabrication [1]. Pedestrian timber bridges can be made quite slender due to light live loads and the high ratio between the modulus of elasticity (MOE) and density. These bridges can therefore be prone to disturbing vibrations. For instance, a serviceability study of the Góis footbridge in [2] showed that some peak accelerations exceeded the limit values and the Lardal footbridge in Norway was reported to experience very high lateral accelerations [3].

A higher vibration response will occur if the pedestrian step frequencies (1–3 Hz in the Eurocode [4]) are coincident with a natural frequency of a bridge. In the Eurocode, bridges with natural frequencies below 5 Hz (vertical modes) and below 2.5 Hz (lateral and torsional modes) require a dynamic analysis to ensure that comfort requirements are fulfilled [5]. The Sétra guideline states similar requirements [6]. It is therefore important to have sufficiently accurate design values of the natural frequencies and damping ratios to ensure good comfort of the bridge.

Damping for timber bridges can be set to 1% without and 1.5% with mechanical joints according to Eurocode [7] and 1% for dynamic calculations according to Sétra [6] which can be regarded as quite conservative. Several previous studies have investigated the dynamic properties of pedestrian timber bridges [2,8–12] and the damping ratios range between 0.2–4.5% in these studies with the most common values around 1–3%. The damping ratio is reported to be higher if an asphalt layer is added to the bridge [11,13]. It is also reported that elastomers at the bridge supports could induce more damping to the structure [14].

Previous studies have implemented finite element (FE) models of timber footbridges [8–10,15,16]. These studies show that it is difficult to get an accurate model without calibrating the model to experimental results. The connections between different construction elements are an important issue. An updated FE model considering the stiffness from steel joints proved to be an important modelling aspect in [10]. The connections between different details such as crossbeams and deck as well as the effect of varying boundary conditions (BCs) were

* Corresponding author.
E-mail address: jbergenu@kth.se (J. Bergenudd).

https://doi.org/10.1016/j.engstruct.2022.115429
Received 2 June 2022; Received in revised form 9 November 2022; Accepted 4 December 2022
Available online 6 January 2023
0141-0296/© 2022 The Author(s). Published by Elsevier Ltd. This is an open access article under the CC BY license (http://creativecommons.org/licenses/by/4.0/).

Fig. 1. The bridge viewed from the side.

shown to affect the results to a great extent in [8]. The stiffness of the railings could also be important to consider in design of slender footbridges [14].

Previous studies have investigated the effect of asphalt on pedestrian timber bridges [8,11–13]. Two scale models were constructed in [13] where numerical and experimental results were presented with and without an asphalt layer. The results correlate with [11] and show that the damping is increased and the natural frequencies are decreased by adding an asphalt layer at room temperature. The results in [11,13] show that full shear transfer between the asphalt and the timber in the FE models should be considered. The temperature effects from the viscoelastic properties of the asphalt layer were investigated in [11]. The study show that the resonance frequencies increase at lower temperatures and that the damping ratios are similar at warm and cold conditions for two footbridges [11].

Structural health monitoring has also previously been carried out in studies such as [17] where it was showed that the first lateral mode decreased due to decay of the timber bridge. Previous studies also present linear variations of the MOE of timber based on the moisture content and temperature [18,19]. These studies also implement a viscoelastic material model for timber and show that the MOE and consequently the natural frequencies vary throughout the lifespan of the bridge. However, in the present work the long-term variations of the properties of the bridge during its lifetime are not considered.

In this article, a bridge in Växjö, Sweden, is dynamically tested at four different construction stages to investigate the influence of adding the railings and the asphalt layer. The temperature effects for the finished bridge are also evaluated. Experimental resonance frequencies and damping ratios are determined for each construction stage. The main objective is thereafter to implement FE models for each construction stage and calibrate them against the experimental results with sufficient accuracy. This will hopefully increase the general understanding of how to properly model the different parts for pedestrian timber bridges.

2. The bridge

The bridge is situated in Växjö, Sweden, and is a 26.1 m long bridge in total with a single span of 25 m, see Fig. 1. The main structure consists of five longitudinal beams (165 × 1170 mm) with a stress-laminated timber (SLT) deck inserted between the beams at the top, see Fig. 2. The c/c between the longitudinal beams is 890 mm and the total width of the SLT deck is 4005 mm. The SLT deck consists of 22 planks, where 18 pieces have a cross-section of 140 × 315 mm and 4 pieces of 165 × 315 mm. The 4 larger pieces are situated precisely at the middle between the longitudinal beams. Pre-stressing of the SLT deck is achieved with 43 steel bars (Ø20 × 4935 mm) running through the mid-height of the SLT deck. The first position of these steel bars is 450 mm from the bridge deck boundaries with a c/c of 600 mm along the bridge longitudinal axis. Crossbeams (115 × 540 mm) are constructed directly underneath the SLT deck between the longitudinal beams. The first position of the crossbeams is 1050 mm from the bridge deck boundaries and are thereafter positioned with a c/c of 6 m symmetrically along the bridge longitudinal axis. Steel bars (Ø20 × 3746 mm) are located at the same longitudinal positions as the crossbeams but 210 mm from the longitudinal beams' lower edge. All load-bearing timber parts are made out of glued laminated timber with quality GL 30c.

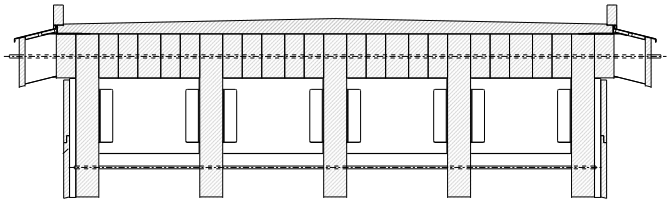

Fig. 2. The bridge cross-section.

2.1. Bridge supports

The supports are identical at both boundaries and for all individual beams, see Fig. 3. The only difference is that the bolt holes are circular on one side and oval on the other side to allow for expansion and shrinkage due to temperature and moisture. The longitudinal beams rest on plastic pads (20 × 165 × 240 mm) made of high-density polyethylene (HDPE or PEHD) and is named PEHD-1000 by the manufacturer. The plastic pads are put in place at construction stage 1 and remain there throughout the lifespan of the bridge. On the sides of the beams, steel plates (12 × 150 × 550 mm) are inserted approximately 300 mm into the concrete. The steel plates on the sides are connected to each other with a bolt and a PEHD-1000 pad exists between the steel plates and the beams. The bridge support is symmetrically constructed around the centerline in the figure. The centerline is located 550 mm from the ends of the longitudinal beams.

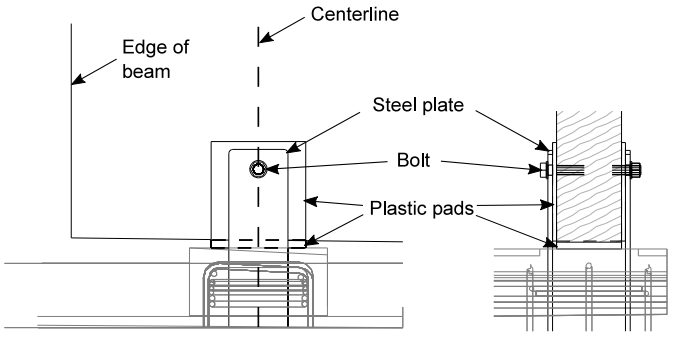

Fig. 3. Bridge supports.

Fig. 4. The finished bridge with railings and asphalt.

2.2. Railings

The bridge is constructed with railings that are continuous beyond the bridge deck with 7.65 m on both sides, see Fig. 4. The railings are bolted into the concrete foundation at 5 locations on each boundary edge (20 connections in total). The railings are attached on 14 locations on each side of the bridge deck. The attachments consist of steel plates bolted into the bridge deck. The total weight of the railings on the bridge deck (not including the railings at the continuity) is around 2.2 tonnes.

2.3. Asphalt

A preliminary mastic asphalt layer is constructed on the bridge with a constant thickness of 75 mm. The final asphalt layer with camber seen in Fig. 2 is not established at the time of the experiments. The asphalt is denoted PGJA 11 in the Swedish norm with a nominal maximal aggregate size of 11 mm and polymer modified bitumen. The asphalt has a 300 mm continuity beyond the bridge ends at each side.

3. Dynamic experiments

3.1. Construction stages

The experiments were performed at four construction stages:

1. Timber structure consisting of longitudinal beams, SLT deck and crossbeams.
2. Timber structure and railings.
3. Timber structure, railings and asphalt during warm conditions.
4. Timber structure, railings and asphalt during cold conditions.

3.2. Equipment

Nineteen accelerometers of type PCB 393A03 with sensitivity 1 V/g were installed at the bridge deck. Two accelerometers of type PCB 393B31 (10 V/g) were installed at the bridge supports. Transient impulse forces of around 10 kN was achieved with a Dytran impulse hammer model 5803A. Slow sine testing was achieved with an electrodynamic shaker of type BD-5 from Wölfel Monitoring Systems. The electrodynamic shaker applied a force of 75 N and a linearly increasing frequency of 1 Hz/min. The asphalt temperature was estimated with an infrared thermometer of type Testo 830-T2.

3.3. Instrumentation

The same instrumentation setup was implemented at the four construction stages, see the bridge from above in Fig. 5. The setup consisted of 14 vertical (a_{V1}–a_{V14}) and 5 lateral (a_{L1}–a_{L5}) accelerometers at the bridge deck as well as 2 axial (or longitudinal) accelerometers (a_{A1}–a_{A2}) at the bridge supports. The excitation was applied at 6 points: 5 vertical (E1–E5) and 1 lateral (E6) were chosen in order to identify as many modes as possible. Hammer excitation was applied at each excitation point whereas slow sine testing was only applied at E2 and E5 to capture the first bending and torsional modes. Approximately 10 hammer hits were recorded at each excitation point in order to average the frequency response functions (FRFs).

4. Modal parameter extraction

The post-processing consisted of producing FRFs using the H_1-estimator which assumes that noise only exists in the output signal [20]. Two different curve-fitting methods were thereafter applied to extract the modal parameters.

4.1. Least-squares complex exponentials method

The least-squares complex exponentials (LSCE) method estimates modal parameters based on impulse response functions. The parameters extracted by this method approximate the FRFs on pole-residue form with the Laplace variable (s). The receptance function based on displacement (X) and force (F) for accelerometer i and excitation point j summarized for P number of poles (s_n) and residues ($_nR_{ij}$) can be seen in Eq. (1). Information about the LSCE method can be found in literature [21,22].

$$H_{ij}(s) = \frac{X_i(s)}{F_j(s)} = \sum_{n=1}^{P}\left(\frac{{}_nR_{ij}}{s-s_n} + \frac{{}_nR^*_{ij}}{s-s^*_n}\right) \tag{1}$$

4.2. Single degree of freedom method

The single degree of freedom (SDOF) method approximates each resonance peak individually in the FRFs as an SDOF oscillating mass–spring–damper system. The modal parameters are obtained by polynomial curve-fitting of the accelerance function based on acceleration (A) and force (F) expressed with the stiffness (k), angular frequency (ω), natural frequency (ω_n) and damping ratio (ζ), see Eq. (2).

$$|H(\omega)| = \left|\frac{A(\omega)}{F(\omega)}\right| = \frac{\omega^2/k}{\sqrt{\left(1-\left(\frac{\omega}{\omega_n}\right)^2\right)^2 + \left(2\zeta\frac{\omega}{\omega_n}\right)^2}} \tag{2}$$

5. Material properties

5.1. Timber

The material parameters for GL 30c provided by the European standard [23] are initially applied in the FE model. Tuning of these material parameters is performed in a later stage in order to use values closer to Norway spruce (*Picea abies* L.), which is the timber used for the bridge, and to get better agreement with the experimental results. Two previous studies were used to get reasonable values of the dynamic MOE in the fibre direction ($E_{0,dyn}$) and density (ρ), see Table 1. In both studies dynamic tests on specimens of Norway spruce were conducted. The Scandinavian company Moelven tested 155 beams with quality CE L40c (equivalent to GL 30c). Jockwer [24] tested 46 specimens with quality CE L40c. The moisture content was close to the reference value of 12% [23] in both studies. The values for the two studies can be seen to be quite similar which reinforces their reliability.

The Poisson's ratios used in the FE model were retrieved from several literature sources [25–29], see Table 2.

5.2. Railings and steel bars

The material parameters of steel for the railings and the bars in the deck are: $E = 210$ GPa, $\rho = 7850$ kg/m^3 and $\nu = 0.3$. The upper part of the railings is a U-profile of aluminium with material properties: $E = 70$ GPa, $\rho = 2700$ kg/m^3 and $\nu = 0.3$.

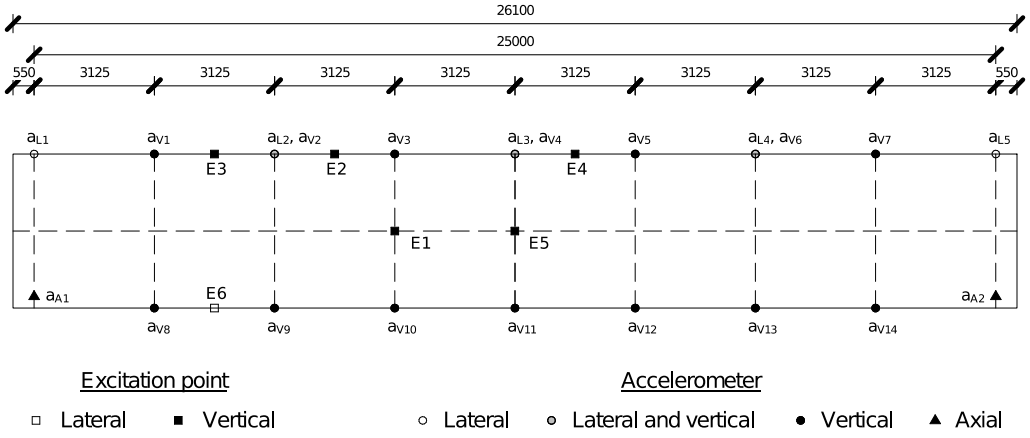

Fig. 5. Instrumentation setup.

Table 1
Material properties from the studies by Moelven and Jockwer [24]. Number of samples (n), mean value (μ) and coefficient of variation (CoV).

Study	n [−]	ρ		$E_{0,dyn}$	
		μ [kg/m^3]	CoV [−]	μ [MPa]	CoV [−]
Moelven	155	470.4	0.032	12299.5	0.057
Jockwer	46	480.2	0.068	12706.3	0.184
Total	201	472.6	0.044	12392.6	0.103

Table 2
Poisson's ratios for the timber. L: Longitudinal. R: Radial. T: Tangential.

ν_{LR}	ν_{LT}	ν_{RT}
0.49	0.49	0.42

Table 3
Estimated material properties for the asphalt layer during the warm and cold experiments (stage 3 and 4).

Stage	T [°C]	ν [−]	ρ [kg/m^3]	E [GPa]
Stage 3	40	0.4	2450	1
Stage 4	0	0.2	2450	17

5.3. Asphalt

The estimated material properties for the asphalt layer during the warm and cold measurements (stage 3 and 4) are presented in Table 3. The density for asphalt is typically between 2400–2500 kg/m^3 [1,30–32]. The MOE is retrieved from experimental studies of stone mastic asphalt such as [33–35] since no studies could be found for mastic asphalt. Stone mastic asphalt is similar to mastic asphalt but usually has a higher aggregate content and lower bitumen content. The studies show similar results for the resilient modulus (S_m) and dynamic modulus of elasticity (E^*).

The Poisson's ratio is estimated from a study [36] that performed laboratory tests with dynamic cyclic loading of asphalt at different frequencies and temperatures resulting in a complex Poisson's ratio (ν^*). Similar values were obtained in [37].

5.4. Plastic pads

The plastic pads at the bridge supports are not included in the FE model. However, as it will be shown in Section 8.2, longitudinal springs have to be applied at the supports in order to calibrate the model. If these springs are entirely due to the shear deformation of the pads then their stiffness k_s can be obtained as follows. The MOE of the plastic pads is 750 MPa as given from the manufacturer, which is similar to other sources for high-density polyethylene [38]. The Poisson's ratio is set to 0.45 [38,39] which gives a value of 260 MPa for the shear modulus (G). The area and the thickness of the pad are: $A = 165 \times 240$ mm and $t = 20$ mm. x is the longitudinal displacement of the upper side of the pad. Then the shear strain (γ) and shear force (V) are defined according to Eq. (3), giving a spring stiffness $k_s = 510$ MN/m.

$$V = AG\gamma = AG\frac{x}{t} = k_s x \tag{3}$$

6. Finite element modelling

The finite element (FE) model, see Fig. 6, implemented in the commercial software Abaqus, is described in this section.

6.1. Material modelling

An orthotropic elastic material is used to model the timber deck. The constitutive relation shown in Eq. (4) (see Box I) is used, where L, T and R refer to the longitudinal (parallel to the fibres), tangential and radial directions of the timber. The values of E_L (E_0), $E_R = E_T$ (E_{90}), $G_{LT} = G_{LR}$ (G_0) and G_{RT} (G_{90}) are given in Table 7. The values of ν_{LR}, ν_{LT} and ν_{RT} are given in Table 2. The remaining Poisson's ratios are then calculated using the relation $\nu_{ij}/E_i = \nu_{ji}/E_j$, where $\nu_{ij} = -\varepsilon_j/\varepsilon_i$. The linear elastic material behaviour is defined with "Engineering constants" in Abaqus. A material orientation is then assigned to the timber structural parts as follow: for the deck, E_L is in the longitudinal direction of the bridge; for the crossbeams, E_L is in the transversal direction of the bridge. Additional information about the orthotropic material properties of timber can be found in [40].

6.2. Mesh

The deck and longitudinal beams are modelled with 20-node solid elements (C3D20) with a mesh size of approximately 100 mm. The crossbeams and railings are modelled with 4-node shell elements (S4R) with a mesh size of approximately 50 and 75 mm respectively. The asphalt is modelled with the same element type as the timber deck. The asphalt layer is divided into four equally thick layers and has an approximate element size of 100 mm. The bars located at the main beam lower edges are modelled with 2-node cubic beam elements (B33) with a mesh size of approximately 50 mm.

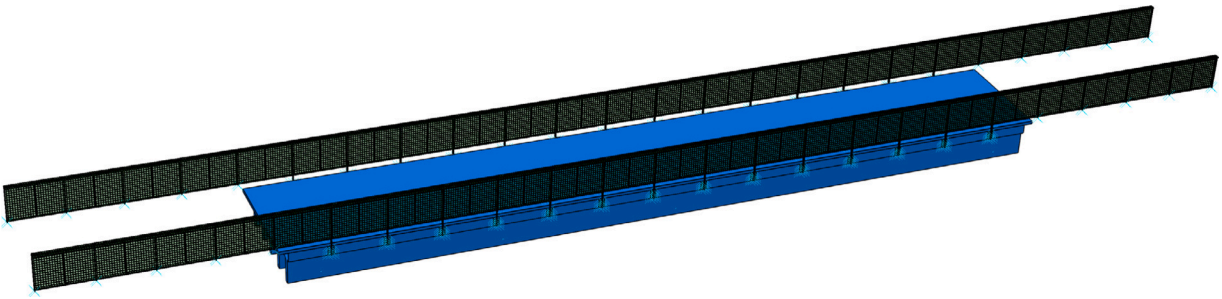

Fig. 6. Finite element model.

$$\begin{pmatrix} \varepsilon_{LL} \\ \varepsilon_{RR} \\ \varepsilon_{TT} \\ \gamma_{RT} \\ \gamma_{LT} \\ \gamma_{LR} \end{pmatrix} = \begin{pmatrix} 1/E_L & -\nu_{RL}/E_R & -\nu_{TL}/E_T & 0 & 0 & 0 \\ -\nu_{LR}/E_L & 1/E_R & -\nu_{TR}/E_T & 0 & 0 & 0 \\ -\nu_{LT}/E_L & -\nu_{RT}/E_R & 1/E_T & 0 & 0 & 0 \\ 0 & 0 & 0 & 1/G_{RT} & 0 & 0 \\ 0 & 0 & 0 & 0 & 1/G_{LT} & 0 \\ 0 & 0 & 0 & 0 & 0 & 1/G_{LR} \end{pmatrix} \begin{pmatrix} \sigma_{LL} \\ \sigma_{RR} \\ \sigma_{TT} \\ \tau_{RT} \\ \tau_{LT} \\ \tau_{LR} \end{pmatrix} \tag{4}$$

Box I.

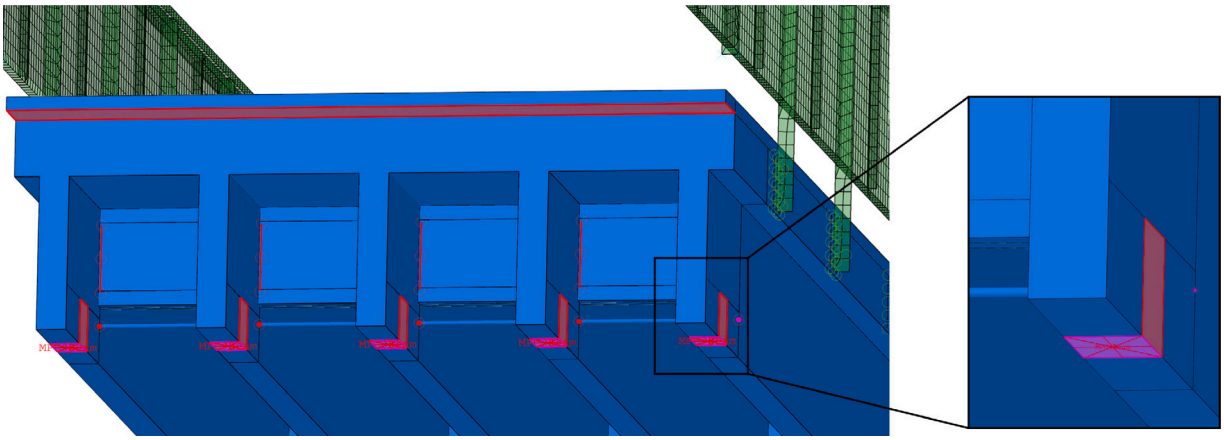

Fig. 7. Finite element model – boundary conditions and constraints.

6.3. Boundary conditions

Multi-point constraints (MPCs) are used to model the supports at each longitudinal beam. A reference point at the interface between the plastic pad and longitudinal beam is connected to the surface at the bottom of the beam with the rigid beam formulation in Abaqus, see Fig. 7. Boundary conditions (BCs) are applied at the reference points as either free (F) or pinned (P). Both BC types restrict vertical and lateral translations but P also restricts longitudinal translation whereas F sets it free. The steel plates on the beam's sides are assumed to only restrict lateral movement. This effect is modelled by introducing BCs on the side of the beams, see Fig. 7. The railings are assumed to be restricted in all degrees of freedom on the boundary edge since they are bolted rigidly into the concrete foundation. The asphalt is modelled both with and without the continuity at the ends of the bridge, see the surface of the continuity in Fig. 7. Pinned BC are applied at this surface.

6.4. Additional mass

The pre-stressed steel bars in the timber deck are added as a volume proportional non-structural mass. In the FE models, the asphalt is only considered as additional mass were two methods are applied: volume proportional non-structural mass and a shell layer using 4-node surface elements without stiffness (SFM3D4). The total mass of the protecting wood panel on the sides, the angle iron connections at the crossbeams and the additional parts for the pre-stressing of the SLT deck only contributes with a few percent of the total mass of the bridge and is therefore omitted from the model.

6.5. Constraints

Tie constraints are used to connect the crossbeams, steel bars and railings to the timber deck, see Fig. 7. The asphalt layer, both for the solid and shell models, is fully connected to the deck with a tie constraint at the interface between the asphalt and timber. The asphalt shell layer with surface elements is located at the centre of gravity of the real asphalt layer.

6.6. Railings

The railings are modelled using shell elements. All the parts are modelled realistically except for the safety net, see Fig. 4. The properties of the shell elements representing the safety net are not trivial and are calibrated to be in agreement with the experimental results.

Table 4
Average air temperature (T) and relative humidity (RH) during the experiments.

Property	Stage 1	Stage 2	Stage 3	Stage 4
T [°C]	12.6	5.5	21.4 (41.9[a])	−0.8 (0.6[a])
RH [%]	57	48	58	70

[a]Average temperature of the asphalt layer.

Table 5
Experimental resonance frequencies.

Stage	Resonance frequencies [Hz]					
	B1	T1	T2	L1	B2	T3
Stage 1	4.93	5.24	7.11	9.65	13.41	14.37
Stage 2	5.03	5.31	7.16	9.65	13.52	14.56
Stage 3	4.07	4.52	6.33	9.81	10.52	12.72
Stage 4	4.74	5.58	8.05	11.45	12.37	14.54

To achieve that, the density and the thickness are changed according to $t = m/A\rho$ while keeping the mass and the area of the net constant.

In order to greatly reduce the computational time and to avoid local modes for the railings, substructure modelling is employed. The railings are modelled separately and only the nodes connecting the railings to the bridge deck and the nodes at the railing's BCs at the continuities are kept for the main analysis. Solving the substructure for 20 eigenmodes was sufficient for convergence.

7. Experimental results

The average temperature and relative humidity during the experiments are presented in Table 4. The resonance frequencies and damping ratios from the experiments are presented in Table 5 and Table 6 respectively. These are average values based on all excitation points and accelerometers. Both modal parameter extraction methods are applied and they give similar results [41]. The modes of vibration are abbreviated according to their shape with B (bending), L (lateral, i.e. in the transverse direction of the bridge) and T (torsion) as well as being ordered numerically (1, 2, ..., n) within their subcategory. An example of an experimental FRF at stage 1 can be seen in Fig. 8 for excitation point E2 and accelerometer a_{V3}. All vertical modes between 0–15 Hz are clearly seen in the plot.

7.1. Stage 2: Railings

The resonance frequencies are increased with around 0–2% at stage 2 compared to stage 1. At stage 1, some parts of the railings are present on the bridge, see Fig. 9. They contribute with around 5% of the total mass of the bridge at stage 1. Without the mass of the railings, the experimental resonance frequency for the first bending mode at stage 1 would have been approximately $f = 4.93 \cdot \sqrt{1.05} = 5.05$ Hz, which is very close to the value at stage 2. The total railing structure contributes to around 10% of the bridge's total mass at stage 2. It can therefore be concluded that the railings must increase the stiffness of the bridge with around 10%.

7.2. Stage 3: Asphalt (warm conditions)

The vertical resonance frequencies are decreased around 10–20% when the asphalt layer has been installed at warm conditions. The average temperature of the asphalt layer is around 42 °C and has a very low MOE at this temperature, see Table 3. The stiffness is therefore only slightly increased but the mass of the bridge is increased with a factor of 2. The resonance frequency for the first lateral mode is increased. This is most likely due the asphalt layer's second moment of area which is a factor $3 \cdot 10^3$ larger in the lateral compared to the vertical direction.

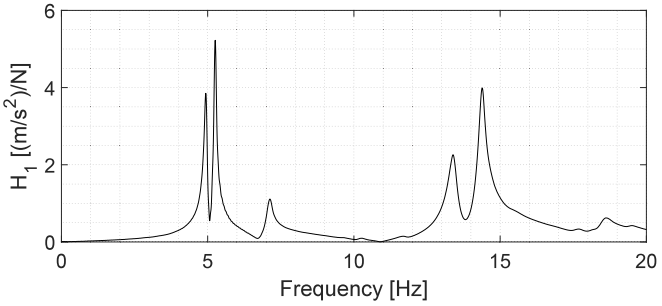

Fig. 8. Experimental frequency response function at stage 1.

Fig. 9. Side view of the bridge at stage 1. The vertical flat bars and steel plates for the railings are present on the bridge.

7.3. Stage 4: Asphalt (cold conditions)

The vertical resonance frequencies are increased around 15–30% at cold conditions which is mainly due to the increase in the asphalt's MOE at cold temperatures.

7.4. Damping

The damping ratios for the finished bridge are around 2–3%, see Table 6. They can be seen to be in the normal range of 1–3% reported in previous literature for pedestrian bridges [8,9,42]. The damping is increased for all construction stages. Friction at the joints and connections as well as material damping for the railings is probably the main reason for the increase in damping at stage 2. The asphalt viscoelastic material properties as well as possible friction at the bridge deck interface is probably the main reason to the increase in damping at stage 3 and 4. The damping value for the second torsional mode is very high at stage 3 which cannot be fully explained.

8. Numerical results

8.1. Modes of vibration

The first six modes in the FE model and from the experiments can be seen in Fig. 10. The first two bending modes (B1–B2), first three torsional modes (T1–T3) and the first lateral mode (L1) are captured.

8.2. Stage 1: Timber structure

The FE model is firstly calibrated for stage 1 where the steel plates and vertical flat bars for the railings, see Fig. 9, are added as point masses of around 34 kg each. Material properties according to European standard [23] are initially applied for the timber deck. The BC combinations F-F, P-F and P-P are tested, where P-F for example denotes applying P at one support and F at the other, see Section 6.3.

Table 6
Experimental damping ratios presented as average and standard deviation, μ (σ).

Stage	Damping ratios [%]					
	B1	T1	T2	L1	B2	T3
Stage 1	1.04 (0.13)	0.88 (0.08)	1.47 (0.02)	1.16 (0.02)	1.17 (0.12)	0.84 (0.03)
Stage 2	1.37 (0.21)	1.10 (0.13)	1.96 (0.12)	1.27 (0.03)	1.57 (0.14)	0.88 (0.05)
Stage 3	1.96 (0.17)	2.03 (0.17)	4.85 (0.22)	1.97 (0.04)	1.72 (0.09)	1.90 (0.05)
Stage 4	2.65 (0.17)	2.97 (0.24)	2.66 (0.27)	2.52 (0.23)	2.59 (0.19)	2.12 (0.17)

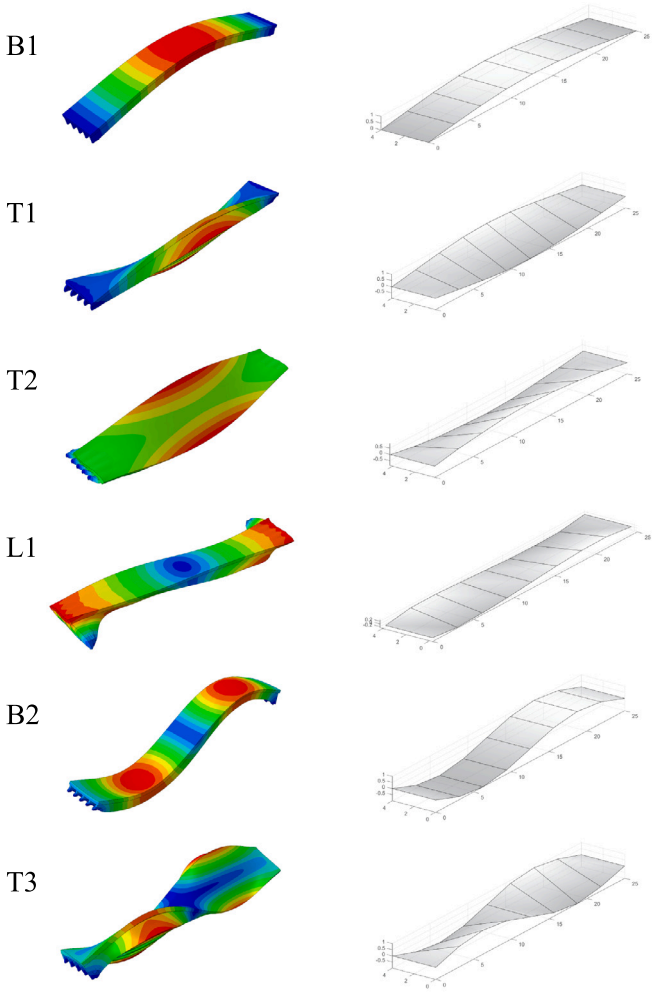

Fig. 10. First six modes of vibration. Left: Numerical. Right: Experimental.

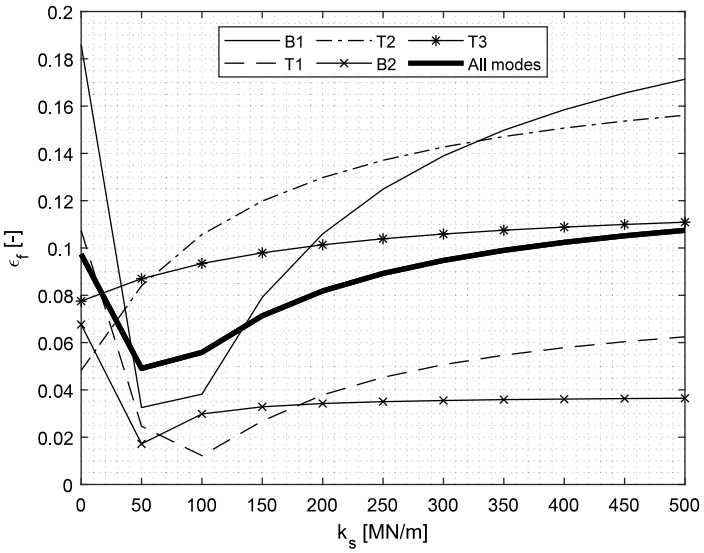

Fig. 11. Calibration of the longitudinal springs. $\epsilon_f = \left|\frac{f_{num} - f_{exp}}{f_{exp}}\right|$.

The results are presented in Table 7. It can be observed that the results with F-F and P-F are far from the experimental results for B1 and no possible combination of E_0 and ρ with reasonable values can generate better results. In addition, with F-F and P-F the numerical results for B1 are lower than the experimental values but the opposite applies for B2. Then, it seems that the only modelling option to get results closer to the experimental values is to consider that the plastic pads at the supports introduce some longitudinal stiffness. For that, BCs are set to F-F and longitudinal springs are introduced at the BCs.

A parameter study where the spring stiffness varies from 0 to 500 MN/m is presented in Fig. 11. The error for L1 is out of range compared to the values for the other modes and is therefore not included in the figure. B1, T1 and B2 reach a minimum at around 50–100 MN/m.

The results (Cal. 1) with a spring stiffness of 50 MN/m are shown in Table 7. A tuning of the material parameters (Cal. 2) is thereafter performed in order to get results closer to the experimental values. For that, a model updating procedure is performed. The material parameters in Table 7 are calibrated by minimizing the error between the experimental and numerical natural frequencies. The optimal parameters are very close to the material properties in Table 1. It can be observed that the obtained spring stiffness (85 MN/m) is much lower than the theoretical value (510 MN/m) in Section 5.4 by assuming only shear deformation of the plastic pads. It can therefore be concluded that some gliding between the plastic pads and longitudinal timber beams occurs. All resonance frequencies in "Cal. 2" are very close to the experimental values except for L1. This is probably due to the fact that the lateral BCs representing the steel plates are too conservative. In the following sections the final material values from "Cal. 2" in Table 7 are used.

8.3. Stage 2: Railings

Three different approaches are tested for stage 2, see Table 8:

1. *No railing mass*: The calibrated FE model from stage 1 (Cal. 2) but without the point masses for the parts of the railings present at stage 1, see Fig. 9.
2. *Point mass*: Point masses (78 kg) are added at each location of the railing's attachments to the bridge deck.
3. *Railings (calibrated)*: Realistic model of the railings, see Section 6.6 and Fig. 6. The obtained calibrated thickness of the safety net is $t = 0.05$ mm.

The first approach gives results close to the experimental values, which shows that it is possible to omit the railings from the FE model. Less accurate results are obtained for the second approach where only the mass of the railings is considered. In the third approach, a detailed model of the railings is implemented where the stiffness of the safety net is the main uncertainty. The shell thickness for the safety net is

Table 7
Calibration at stage 1. Results for the different boundary conditions (F-F, F-P and P-P) as well as the first (Cal. 1) and second calibration (Cal. 2).

Model	Natural frequencies [Hz]						Material parameters					
	B1	T1	T2	L1	B2	T3	E_0 [MPa]	ρ [kg/m^3]	G_0 [MPa]	E_{90} [MPa]	G_{90} [MPa]	k_s [MN/m]
Exp.	***4.93***	***5.24***	***7.11***	***9.65***	***13.41***	***14.37***						
F-F	4.13	4.69	7.64	13.37	14.75	15.49	13000	430	650	300	65	0
P-F	4.09	5.31	7.97	14.23	14.29	15.69			"			"
P-P	5.79	6.34	8.58	14.36	14.70	16.13			"			"
Cal. 1	4.89	5.14	7.87	13.87	14.10	15.59			"			50
Cal. 2	4.93	5.10	7.11	12.59	13.42	14.53	12600	460	725	125	75	85

Table 8
Results from the FE models for construction stages 1–4. All values are in hertz (Hz).

Stage	Pre-conditions	B1	T1	T2	L1	B2	T3
Stage 1	Exp.	***4.93***	***5.24***	***7.11***	***9.65***	***13.41***	***14.37***
	Cal. 2	4.93	5.10	7.11	12.59	13.42	14.53
Stage 2	Exp.	***5.03***	***5.31***	***7.16***	***9.65***	***13.52***	***14.56***
	No railing mass	5.03	5.29	7.36	12.85	13.68	15.28
	Point mass	4.81	4.88	6.83	12.23	13.03	13.60
	Railings (calibrated)	5.03	5.24	6.93	12.36	13.58	13.92
Stage 3	Exp.	***4.07***	***4.52***	***6.33***	***9.81***	***10.52***	***12.72***
	Only mass (non-structural mass)	3.82	4.03	5.36	9.52	10.28	11.19
	Only mass (surface layer)	3.82	4.32	5.08	9.20	10.25	11.75
	Asphalt layer	3.85	4.47	5.20	9.36	10.35	12.04
	Asphalt layer (continuity)	4.36	5.03	9.15	–	11.93	12.75
Stage 4	Exp.	***4.74***	***5.58***	***8.05***	***11.45***	***12.37***	***14.54***
	Asphalt layer	4.20	4.95	5.98	9.65	11.20	13.57
	Asphalt layer (continuity)	4.97	6.30	15.12	–	13.11	14.62

therefore calibrated such that the numerical results agree with the experimental values. It can also be noted that removing the parts of the railings beyond the bridge ends decreases the natural frequencies with less than 1%. The third approach, i.e. the calibrated model of the railings, is applied in the FE models at stage 3 and 4.

8.4. Stage 3: Asphalt layer (warm conditions)

The following approaches are considered for modelling the asphalt at warm conditions, see Table 8:

1. *Only mass (non-structural mass)*: The asphalt is added as a volume proportional non-structural mass to the timber deck.
2. *Only mass (surface layer)*: The asphalt is modelled with a shell layer of surface elements, see Section 6.4.
3. *Asphalt layer*: The asphalt is modelled with solid elements and using the material values in Table 3.
4. *Asphalt layer (continuity)*: Same as (3) but also including the asphalt continuity at the bridge boundaries.

The three first approaches give almost the same results for the two bending modes whereas differences can be observed for the torsional modes, see Table 8. The second approach gives relatively accurate results compared to the experiments and seems therefore to be an appropriate way to model the asphalt. The results for the third approach are lower than the experimental values (5% for B1). Several alternatives are tested in order to increase B1 to the experimental value. The first one is to increase the MOE of the asphalt to 10 GPa which is an unrealistic value at this temperature. The second one is to increase the spring stiffness at the supports to $2k_s$, but the accelerometers at the bridge supports show that the mode shape amplitude at the bridge supports is similar for all construction stages. The third alternative is to introduce the continuity of the asphalt layer (approach 4), see Table 8. The obtained results are too high but they show that the continuity of the asphalt may have an impact of the overall stiffness of the bridge.

8.5. Stage 4: Asphalt layer (cold conditions)

The following approaches are considered for modelling the asphalt at cold conditions, see Table 8:

1. *Asphalt layer*: The asphalt is modelled with solid elements and using the material values in Table 3.
2. *Asphalt layer (continuity)*: Same as (1) but also including the asphalt continuity at the bridge boundaries.

The difference in the results for the first approach compared to the experimental values are around 10% for all modes except T2 which could be considered as acceptable. As for the previous section, the results with the second approach are too high but show that the continuity of the asphalt layer beyond the bridge ends adds to the stiffness of the bridge.

9. Conclusions

This article presents experimental results from in-situ dynamic testing of a pedestrian timber bridge at four construction stages: (1) on only the timber structure, (2) on the timber structure with the railings, (3) on the timber structure with railings and an asphalt layer during warm conditions and (4) same as stage 3 but during cold conditions. The bridge is 26.1 m long in total and has a single span of 25 m. The main load-bearing structure consists of five longitudinal glued laminated timber beams with an SLT deck and asphalt layer on top. FE models for the construction stages are thereafter implemented and calibrated against the experimental results.

The following conclusions regarding the modelling of the different parts of the bridge can be derived:

- The numerical results at stage 1 show that simple boundary conditions at the supports are not sufficient and that longitudinal springs need to be introduced in order to get accurate results. However, the value of the stiffness for these springs cannot be obtained by considering the shear deformation of the plastic pads and is therefore not obvious to determine without experimental results. Further studies could investigate the partial gliding and deformation of the plastic pads in order to predict the stiffness of the springs.
- The experimental results at stage 2 show that the railing structure contributes to 10% of both the stiffness and the mass of the bridge. Consequently, the railings could be disregarded and should not be considered as only an additional mass.

- The results in stages 3 and 4 show that the natural frequencies of the bridge increase with 15–30% between warm and cold conditions. In warm conditions the asphalt can be modelled as just an additional mass by using a shell layer with surface elements. In cold conditions the stiffness of the asphalt cannot be neglected and the asphalt layer can be modelled using solid elements tied to the timber deck surface. However, the numerical values are too low, indicating that some stiffness is lacking. The numerical results show also that the continuity of the asphalt beyond the bridge deck may contribute to the overall stiffness of the bridge.
- The damping ratios increase at all construction stages. They are around 2% at warm conditions (stage 3) and around 2.5% at cold conditions (stage 4).

Some of the conclusions above confirm previous results from the literature, whereas other conclusions can be considered as new knowledge. As already mentioned in previous studies, the present article confirms that it is difficult to model the dynamic behaviour of pedestrian bridges without calibration using experimental results. For the present bridge this difficulty is related to the plastic pads at the supports. It was clear that the deformation of the plastic pads could give some stiffness. But it was not expected that this stiffness would significantly influence the natural frequency of the first bending mode especially for small amplitude of vibrations.

In addition, the present study confirms that the natural frequencies are higher at cold compared to warm conditions, and that it is mainly due to the stiffness of the asphalt. However, the present study shows that the asphalt can be modelled as an additional mass at warm conditions for calibrating the lowest bending mode but not for calibrating the first torsional mode which requires the asphalt to be modelled as a layer on the deck. A new interesting feature in the present work is that the continuity of the asphalt layer beyond the bridge boundaries may have an effect, especially at cold temperatures.

To the authors knowledge, the influence of the railings on the dynamic behaviour of pedestrian timber bridges has not been previously studied experimentally. Structural engineers usually consider the railings as an additional mass but the present work shows that it should not be done for this bridge.

Finally, for the present bridge the damping ratios increase when the asphalt layer has been added to the bridge and are higher in cold compared to warm conditions. This is in line with previous studies. The damping ratios of the completed bridge are higher than the design values of 1–1.5% in Eurocode and 1% in Sétra. This shows the difficulty of picking the damping ratios in the design process of pedestrian timber bridges since damping ratios both lower and higher than the design values can be found from experiments reported in the literature.

CRediT authorship contribution statement

Jens Bergenudd: Conceptualization, Methodology, Software, Formal analysis, Investigation, Writing – original draft, Visualization. **Jean-Marc Battini:** Conceptualization, Writing – review & editing, Supervision, Project administration, Funding acquisition. **Roberto Crocetti:** Conceptualization, Supervision. **Costin Pacoste:** Conceptualization, Supervision.

Declaration of competing interest

The authors declare that they have no known competing financial interests or personal relationships that could have appeared to influence the work reported in this paper.

Data availability

Data will be made available on request.

Acknowledgements

This project is funded by the Swedish Transport Administration and the J. Gustaf Richert foundation. The authors gratefully recognize these contributions. The authors also want to thank the companies Moelven and Skanska for all the help with the dynamic measurements on-site and for providing constructional drawings of the bridge.

References

[1] Swedish Wood. Design of timber structures. Volume 1 - Structural aspects of timber construction. 3rd ed.. Swedish Wood; 2019.
[2] Salgado R, Branco JM, Cruz PJ, Ayala G. Serviceability assessment of the Góis footbridge using vibration monitoring. Case Stud Nondestruct Test Eval 2014;2:71–76. http://dx.doi.org/10.1016/j.csndt.2014.10.001.
[3] Ingólfsson E, Georgakis C, Jönsson J. Pedestrian-induced lateral vibrations of footbridges: A literature review. Eng Struct 2012;45:21–52. http://dx.doi.org/10.1016/j.engstruct.2012.05.038.
[4] Swedish Standards Institute. Swedish Standard SS-EN 1991-2. Eurocode 1: Actions on structures – Part 2: Traffic loads on bridges. 1st ed.. SIS Förlag AB; 2007.
[5] Swedish Standards Institute. Swedish Standard SS-EN 1990. Eurocode – Basis of structural design. 1st ed.. SIS Förlag AB; 2014.
[6] Sétra. Footbridges – assessment of vibrational behaviour of footbridges under pedestrian loading. 2006.
[7] Swedish Standards Institute. Swedish standard SS-EN 1995-2:2004. Eurocode 5: Design of timber structures – Part 2: Bridges. 1st ed.. SIS Förlag AB; 2009.
[8] Neilson JH, Ibisevic A, Ugur H, Battini J-M, Crocetti R, Pacoste C, et al. Experimental and numerical dynamic properties of two timber footbridges including seasonal effects. Int J Civ Eng 2021;19(10):1239–1250. http://dx.doi.org/10.1007/s40999-021-00624-w.
[9] Castro-Triguero R, Garcia-Macias E, Saavedra Flores E, Friswell MI, Gallego R. Multi-scale model updating of a timber footbridge using experimental vibration data. Eng Comput 2017;34(3):754–780. http://dx.doi.org/10.1108/EC-09-2015-0284.
[10] Hawryszków P, Biliszczuk J. Vibration serviceability of footbridges made of the sustainable and eco structural material: Glued-laminated wood. Materials 2022;15(4). http://dx.doi.org/10.3390/ma15041529.
[11] Feltrin G, Gsell S, Steiger R. Temperature effects on the natural frequencies and modal damping of timber footbridges with asphalt pavement. 2011.
[12] Weber B, Feltrin G. Modelling the temperature-dependent dynamic behaviour of a timber bridge with asphalt pavement. In: Excerpt from the proceedings of the 2012 COMSOL conference in Milan. Stockholm: COMSOL; 2012,p. 1–3.
[13] Schubert S, Gsell D, Steiger R, Feltrin G. Influence of asphalt pavement on damping ratio and resonance frequencies of timber bridges. Eng Struct 2010;32(10):3122–3129. http://dx.doi.org/10.1016/j.engstruct.2010.05.031.
[14] Commission E, Centre JR, Goldack A, Trometer S, Keil A, Caetano E, et al. In: Géradin M, Heinemeyer C, Butz C, Sedlacek G, editors. Design of lightweight footbridges for human induced vibrations : Background document in support to the implementation, harmonization and further development of the Eurocodes. Publications Office; 2011, http://dx.doi.org/10.2788/33846.
[15] Rönnquist A, Strømmen E, Wollebæk L. Dynamic properties from full scale recordings and FE-modelling of a slender footbridge with flexible connections. Struct Eng Int 2008;18(4):421–426. http://dx.doi.org/10.2749/101686608786455162.
[16] Altunişik AC, Kalkan E, Okur FY, Şevket Karahasan O, Ozgan K. Finite-element model updating and dynamic responses of reconstructed historical timber bridges using ambient vibration test results. J Perform Construct Facil 2020;34(1):04019085. http://dx.doi.org/10.1061/(ASCE)CF.1943-5509.0001344.
[17] Stiros S, Moschas F. Rapid decay of a timber footbridge and changes in its modal frequencies derived from multiannual lateral deflection measurements. J Bridge Eng 2014;19(12):05014005. http://dx.doi.org/10.1061/(ASCE)BE.1943-5592.0000629.
[18] Fortino S, Hradil P, Koski K, Korkealaakso A, Fülöp L, Burkart H, et al. Health monitoring of stress-laminated timber bridges assisted by a hygro-thermal model for wood material. Appl Sci 2021;11(1). http://dx.doi.org/10.3390/app11010098.
[19] Fortino S, Mirianon F, Toratti T. A 3D moisture-stress FEM analysis for time dependent problems in timber structures. Mech Time-Depend Mater 2009;13(4):333. http://dx.doi.org/10.1007/s11043-009-9103-z.
[20] Brandt A. Noise and vibration analysis: Signal analysis and experimental procedures. Wiley; 2011.
[21] Maia N. Extraction of valid modal properties from measured data in structural vibrations [Ph.D. thesis], University of London; 1988.
[22] Nestorović T, Trajkov M, Patalong M. Identification of modal parameters for complex structures by experimental modal analysis approach. Adv Mech Eng 2016;8(5):1687814016649110. http://dx.doi.org/10.1177/1687814016649110.

[23] Swedish Standards Institute. Swedish standard SS-EN 14080:2013. Timber structures – Glued laminated timber and glued solid timber – Requirements. 2nd ed.. SIS Förlag AB; 2013.
[24] Jockwer R. Structural behaviour of glued laminated timber beams with unreinforced and reinforced notches [Ph.D. thesis], Zürich: ETH-Zürich; 2014, http://dx.doi.org/10.3929/ethz-a-010171641.
[25] Crocetti R, Gustafsson P-J, Danielsson H, Emilsson A, Ormarsson S. Experimental and numerical investigation on the shear strength of glulam. In: Görlacher R, editor. Proceedings of international council for research and innovation in building and construction, working commission W18 - timber structures. Lehrstuhl für Ingeniurholzbau und Baukonstruktion, Universität Karlsruhe; 2010.
[26] Tang L, Yang H, Crocetti R, Liu J, Shi B, Gustafsson PJ, Liu W. Experimental and numerical investigations on the hybrid dowel and bonding steel plate joints for timber structures. Constr Build Mater 2020;265:120847. http://dx.doi.org/10.1016/j.conbuildmat.2020.120847.
[27] Akter ST, Serrano E, Bader TK. Numerical modelling of wood under combined loading of compression perpendicular to the grain and rolling shear. Eng Struct 2021;244:112800. http://dx.doi.org/10.1016/j.engstruct.2021.112800.
[28] Larsson G. High capacity timber joints: Proposal of the shear plate dowel joint, No. 3078 [Ph.D. thesis], LUTVDG/TVSM, Lund University; 2017.
[29] Dahl K. Mechanical properties of clear wood from Norway spruce [Ph.D. thesis], (2009:250). Norwegian University of Science and Technology; 2009.
[30] Baltrušaitis A, Vaitkus A, Smirnovs J. Asphalt layer density and air voids content: GPR and laboratory testing data reliance. Baltic J Road Bridge Eng 2020;15:93–110. http://dx.doi.org/10.7250/bjrbe.2020-15.486.
[31] Sengul CE, Oruc S, Iskender E, Aksoy A. Evaluation of SBS modified stone mastic asphalt pavement performance. Constr Build Mater 2013;41:777–783. http://dx.doi.org/10.1016/j.conbuildmat.2012.12.065.
[32] Chegenizadeh A, Peters B, Nikraz H. Mechanical properties of stone mastic asphalt containing high-density polyethene: An Australian case. Case Stud Construct Mater 2021;15:e00631. http://dx.doi.org/10.1016/j.cscm.2021.e00631.
[33] Zhao Y, Tang J, Liu H. Construction of triaxial dynamic modulus master curve for asphalt mixtures. Constr Build Mater 2012;37:21–26. http://dx.doi.org/10.1016/j.conbuildmat.2012.06.067, Non Destructive Techniques for Assessment of Concrete.
[34] Pokorski P, Radziszewski P, Sarnowski M. Rheological properties of asphalt mixtures for bridge pavements. Procedia Eng 2015;111:637–644. http://dx.doi.org/10.1016/j.proeng.2015.07.060, XXIV R-S-P seminar, Theoretical Foundation of Civil Engineering (24RSP) (TFoCE 2015).
[35] Halle M, Rukavina T, Domitrovic J. Influence of temperature on asphalt stiffness modulus. In: 5th Eurasphalt & eurobitume congress. Istanbul; 2012,p. 13–15.
[36] Gudmarsson A, Ryden N, Di Benedetto H, Sauzéat C, Tapsoba N, Birgisson B. Comparing linear viscoelastic properties of asphalt concrete measured by laboratory seismic and tension–compression tests. J Nondestruct Eval 2014;33(4):571–582. http://dx.doi.org/10.1007/s10921-014-0253-9.
[37] Kim YR, Seo Y, King M, Momen M. Dynamic modulus testing of asphalt concrete in indirect tension mode. Transp Res Rec 2004;1891(1):163–173. http://dx.doi.org/10.3141/1891-19.
[38] hei Nitta K, Yamana M. Poisson's ratio and mechanical nonlinearity under tensile deformation in crystalline polymers. In: Vicente JD, editor. Rheology. Rijeka: IntechOpen; 2012, http://dx.doi.org/10.5772/34881, Ch. 5.
[39] Drai A, Aour B. Analysis of the temperature effect on the behavior of high density polyethylene during high pressure torsion process. In: Society of plastics engineers - EUROTECH 2013. 2013, p. 592–596.
[40] Dinwoodie JM. Timber: Its nature and behaviour. 2nd ed.. London: E. & F. N. Spon; 2000.
[41] Bergenudd J, Battini J-M, Crocetti R, Pacoste C. Study of the dynamic response of a timber pedestrian bridge during different construction stages. In: ICTB 2021 PLUS 4th International Conference on Timber Bridges. Bern University of Applied Sciences; 2022, p. 167–178. http://dx.doi.org/10.24451/gak8-4k79.
[42] Van Nimmen K. Numerical and experimental study of human-induced vibrations of footbridges [Ph.D. thesis], KU Leuven; 2015.